Aerodynamic excitation and sound production of blown-closed free reeds without acoustic coupling: The example of the accordion reed

Denis Ricot[a)]
Laboratoire de Mécanique des Fluides et d'Acoustique, UMR CNRS 5509, Ecole Centrale de Lyon, France

René Caussé and Nicolas Misdariis
Institut de Recherche et Coordination Acoustique/Musique, UMR CNRS 9912, 1 place Igor Stravinsky 75004 Paris, France

(Received 7 February 2003; revised 27 September 2004; accepted 2 December 2004)

The accordion reed is an example of a blown-closed free reed. Unlike most oscillating valves in wind musical instruments, self-sustained oscillations occur without acoustic coupling. Flow visualizations and measurements in water show that the flow can be supposed incompressible and potential. A model is developed and the solution is calculated in the time domain. The excitation force is found to be associated with the inertial load of the unsteady flow through the reed gaps. Inertial effect leads to velocity fluctuations in the reed opening and then to an unsteady Bernoulli force. A pressure component generated by the local reciprocal air movement around the reed is added to the modeled aerodynamic excitation pressure. Since the model is two-dimensional, only qualitative comparisons with air flow measurements are possible. The agreement between the simulated pressure waveforms and measured pressure in the very near-field of the reed is reasonable. In addition, an aeroacoustic model using the permeable Ffowcs Williams–Hawkings integral method is presented. The integral expressions of the far-field acoustic pressure are also computed in the time domain. In agreement with experimental data, the sound is found to be dominated by the dipolar source associated by the strong momentum fluctuations of the flow through the reed gaps.
 [DOI: 10.1121/1.1852546]

PACS numbers: 43.75.Pq [NHF] Pages: 2279–2290

I. INTRODUCTION

The accordion is based on a very old system: the free metal reed which dates from the third millenium BC. It was used in a Chinese musical instrument, the tcheng. Nowadays, this system can be found in the harmonica and the harmonium, for example. The accordion reed is a thin metal plate riveted at one end to a support plate. There is a rectangular slot in the support plate immediately beneath the reed. The aperture is a bit larger than the reed so that the it freely vibrates as a cantilevered beam and does not strike against the support plate. An air flow is generated by the inward or outward movement of the bellows. With regards to Fletcher's classification,[1] the accordion reed is a valve of type $(-,+)$. In the presence of pre-existing flow in the same direction as the instrument, a steady overpressure applied from the upstream side of the reed tends to close the valve and inversely, a steady overpressure applied from downstream of the reed causes it to open further. Of course, if we consider a steady flow in the opposite direction, the valve is of type $(+,-)$. However, in the instrument, the accordion reed only operates in its blown-closed configuration: the inward movement of the bellows generates an upstream steady overpressure P_0 and the outward movement generates a depression on the downstream side of the reed which is equivalent to an upstream overpressure. The self-sustained oscillation results from the unsteady pressure difference between both sides of the reed. But unlike most wind instruments such as woodwind and brass,[2,3] the time-dependent pressure drop is not driven by the oscillation of the air column of a resonator. In the accordion, we can consider that the reed oscillation mechanism and the emitted sound do not depend on the acoustic influence of the upstream and downstream volumes. This kind of oscillating valve can be called a dominant or a strong reed.

In classical reed models[1,2,4] that have been developed for resonator-coupled reeds, the pressure fluctuation $p_{ac}(t)$ is written from the acoustic response of the resonator excited by an unsteady volume flux $q_{ac}(t)$. By assuming the incompressibility of the flow around the reed, the acoustic volume flux at the resonator inlet is matched to the aerodynamic flux through the reed aperture $q_{ac}(t) := q(t) \propto V(t)x_2(t)L$ where $V(t)$ is the flow velocity, $x_2(t)$ is the reed displacement and L is a characteristic length of the orifice. The aerodynamic velocity—and thus the volume flux—is easily calculated from the steady-state Bernoulli equation with a pressure drop $P_0 - p_{ac}(t)$. This modeling approach implicitly supposes that the pressure of the reed flow at the exit of the reed channel exactly equals the acoustic pressure at the entrance of the resonator. This assumption can be justified[5] by noting that a jet is formed at the exit of the reed channel because of the large abrupt transition in cross-sectional area from reed channel to instrument mouthpiece. All the kinetic energy of the flow is supposed to be dissipated in the spreading turbulent

[a)]Current address: 10 avenue Paul Cezanne 78990 Elancourt, France; electronic mail: DenisRicot@aol.com

jet. This hypothesis is also consistent with the modeling of the acoustic source. Indeed, it is clear that only the fluctuating mass is taken for the excitation of the acoustic air column. The fluctuating force associated with the periodic momentum injection can be ignored. Finally, the reed is modeled by a simple mass-spring-damping system. Consequently, a coupled system of three equations (the impedance relation, the Bernoulli equation and the simple harmonic oscillator equation) and three unknown variables $[x_2(t), q(t), p_{ac}(t)]$ can be written. With the same approach, the influence of the internal acoustic impedance of the air supply system (the player's lungs, vocal tract and mouth) can be taken into account.[1] Because of the impedance relation, most calculations are performed in the frequency domain.[1,2] But the frequency–domain approach is not advantageous for strongly nonlinear equations such as the Bernoulli equation. Time–domain solutions[6,4] and hybrid methods[7] have also been proposed.

For a constant surface of contact between the flow and the reed, the dynamic excitation force is a combination of acoustic pressure and pressure induced by velocity variation due to the variation in the aperture area. The velocity-induced pressure fluctuations are found by applying the stationary Bernoulli equation which associates a decrease of the pressure with an acceleration of the fluid. But, without other physical mechanisms such as acoustic feedback, these pressure fluctuations cannot induce self-oscillations. For example, if we suppose a constant volume flow through the reed aperture, it is straightforward to show that the force induced by fluid velocity variation is in phase with the displacement. Energy transfer between the constant supply pressure and the reed oscillation is not possible if we consider only the stationary Bernoulli equation. Titze[8] explained that an asymmetry of the pressure force during the cycle is necessary for reed excitation. In case of resonator-coupled reeds, the pressure asymmetry is provided by the acoustic response of upstream and/or downstream volumes. In case of the accordion reed, there is no acoustic feedback. By supposing that the stationary Bernoulli equation well describes the aerodynamic flow through the reed aperture, other physical mechanisms have been proposed to explain the phase shift of the total force with regard to the reed displacement. For example, a complex evolution of the channel geometry during the cycle can lead to the asymmetry of the total force. This approach is used to model voice production because vocal fold oscillations are not considered to be driven by the acoustic impedance of lungs and vocal tract. Titze[8] used a wave motion model to describe the movement of the tissues and Pelorson *et al.*[9] added a second mechanical oscillator: a phase delay of the total pressure force is obtained because the shape variations of the channel are not the same during closing and opening of the glottis.

The effect of separation and reattachment of the flow in the reed channel has also been studied. Indeed, the flow separation at the inlet of the clarinet reed channel leads to a local acceleration of the flow[5] (vena-contracta effect). Moreover, the total pressure force can also depend on the possible reattachment of the air flow on the reed further in the reed channel. The vena-contracta factor and the location of the reattachment point may vary as a function of the reed position and produce a force in phase with the reed velocity. An example of the modeling of these viscous effects can be found in the study of Pelorson *et al.*[9] At the outlet of the vocal fold channel, he studied the movement of the point where the air flow separates from the glottis. In this case, the total pressure force fluctuates because the reed surface in contact with the unsteady flow fluctuates. Although the consequences of the flow separation are qualitatively and quantitatively significant, it was not shown whether this phenomenon could induce self-oscillation without the presence of the two-mass model.

The separation points of the accordion reed flow are fixed at the sharp edge of the reed. As shown in Sec. II of this paper, there is no flow reattachment on the other side of the reed, therefore the surface of the reed immersed in the flow is constant. The flow separation/reattachment effects are not a candidate for a possible excitation mechanism of the accordion reed.

If we discard the supposition that the unsteady flow can be described by the stationary Bernoulli equation, it appears that the energy transfer from the flow to a free reed can be obtained by two other physical mechanisms. First, the vortex shedding behind a solid obstacle[10] induces a periodic force on the structure. Thanks to their experimental investigations, Saint Hilaire *et al.*[11] concluded that vortex shedding is not responsible for the excitation of his harmonium reed. This result has been also confirmed in a recent study[12] for a blown-open reed.

At last, the inertial effect of the upstream flow has been proposed to be the excitation mechanism of free reeds[11] in the absence of acoustic coupling. The verification of this assumption is one of the purposes of the present work. An analysis of the flow around the accordion reed (Sec. II) shows that the flow can be modeled as an unsteady potential two-dimensional flow. In Sec. III, the aerodynamic force which excites the vibration of the reed is calculated under the incompressible flow hypothesis. From aerodynamic data, a model for the calculation of the aeroacoustic source based on an acoustic analogy is proposed (Sec. IV). Flow and aeroacoustic models are solved in the time domain and results are compared with experimental data (Sec. V). Since the attention of this paper is turned to the analysis of the exact nature of both the excitation force and acoustic source, empirical hypotheses or adjustable parameters must not be used. Because of the complexity of flow equations, the calculation of analytical expressions is only possible with a very simplified representation of the accordion reed. Therefore quantitative values of physical variables are not expected to agree with the actual ones. Only waveforms and spectra are compared to measurements.

II. FLUID MECHANICAL DESCRIPTION OF THE FLOW

The geometry of the accordion reed is slightly different from the reed geometry used by Saint Hilaire *et al.*[11] in their flow visualizations. The initial distance x_0 between the vibrating reed and the support plate is smaller for the accordion reed than for the Saint Hilaire arrangement. The reed is directly riveted onto the support plate, therefore x_0 is very

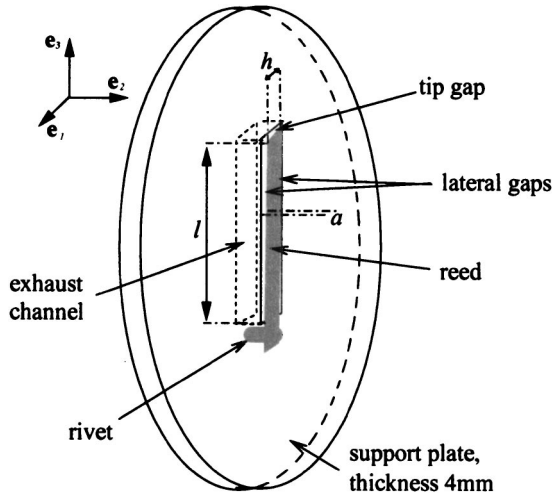

FIG. 1. Sketch of the Plexiglas support plate and riveted reed. The flow is from right to left. The mathematical axes used in the model (Secs. III and IV) are also shown.

small and greatly depends on the stationary profile of the reed. In our case, we can suppose that $x_0 \leqslant 0.4\,\mathrm{mm}$. The thickness of the support plate is another difference. The slot in the support plate will be called the exhaust channel in the following (see Fig. 1). The length of the exhaust channel in the streamwise direction is equal to the thickness of the support plate. We see that this length is quite large compared to the width of the gaps. Therefore a flow reattachment is expected to occur on the lateral walls of the exhaust channel.

In order to check the validity of Saint Hilaire's conclusions concerning the inability of wake instabilities to excite the reed and to have more details on the flow structure, flow visualizations using dye stream injections have been conducted in water. The experimental arrangement is given in Fig. 2. The accordion reed is mounted on a Plexiglas reservoir of about 800 cm^3. The steel reed was $l=32\,\mathrm{mm}$ in length and $b=0.2\,\mathrm{mm}$ in thickness and has a mean width of $h=3.6\,\mathrm{mm}$. In air, the natural frequency of the reed is $f_0=330\,\mathrm{Hz}$. The parameter a is the remaining distance between the reed and the exhaust channel walls when the reed

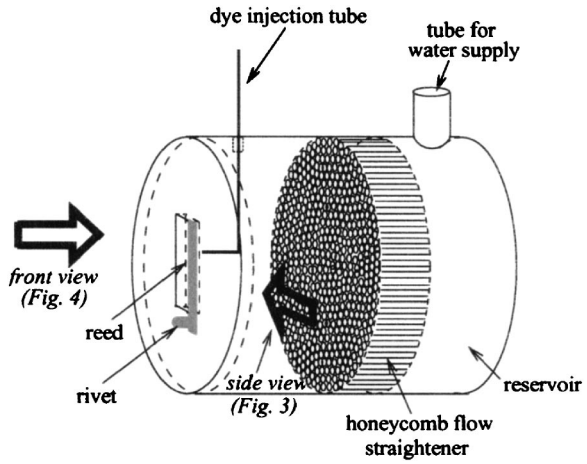

FIG. 2. The experimental setup for water-flow visualizations. This setup is also used for measurements of reed displacement, aerodynamic and acoustic pressures in air flow (Sec. V). The two large arrows indicate the views of the photographs shown in Fig. 3 and Fig. 4.

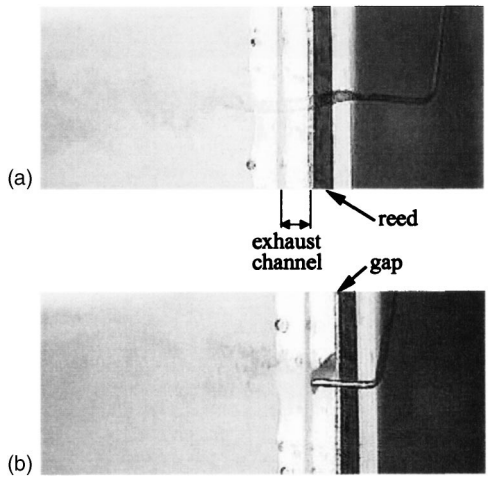

FIG. 3. Side views (see Fig. 2 and Fig. 5) of the flow pattern for two dye stream injection points situated (a) in front of a reed gap, and (b) in the support plate plane. Only a central part of the reed is shown. The supply cavity is on the right. In the upstream region, the dye is convected along potential streamlines. Downstream of the reed, turbulent mixing and diffusion are visible.

is closed. It means that the width of the exhaust channel is $h+2a$. Generally, a is less than 0.2 mm. The notations for the reed dimensions are given in Fig. 1. The reed mounted on its supply cavity is immersed in a discharge tank. The height of the free surface of water in the discharge tank is maintained constant thanks to an overflow pipe. The water was supplied to the reed cavity through a narrow flexible tube from a large supply tank. The average supply pressure of the reed (the difference between the upstream and the downstream pressures) was simply set by varying the distance between the free surfaces of water of the supply and discharge tanks. A honeycomb flow straightener ensures an even upstream flow. This system is visible in the background of the photography given later in Fig. 4. Visualization of the flow field was accomplished by the injection, via a capillary tube, of a dye stream at various locations upstream of the reed.

For a supply pressure of $P_0=2000\,\mathrm{Pa}$, self-sustained oscillations of the reed can be observed. The mean velocity V of the flow through the reed gaps can be evaluated using the stationary Bernoulli equation. The Reynolds number based on the reed width h is about $\mathrm{Re}_h=Vh/\nu\approx 6000$ where ν is the kinematic viscosity of water. For self-sustained oscillations in air at normal playing pressure, the Reynolds number of the flow is slightly inferior to that observed in water but has the same order of magnitude. Thus, we can suppose that the excitation mechanism and the flow characteristics in water are the same as that in air flow. The frequency of reed oscillation under water flow is 142 Hz. The stroboscopic images that are not reported here clearly show that the reed oscillates on the first mode of the cantilever beam. The great difference between the oscillation frequency and the natural frequency of the reed in air is a consequence of the added mass effect of water (see Sec. III C).

Typical flow patterns are shown in Figs. 3(a) and 3(b). As expected, the upstream flow is laminar. The dye is convected along well-defined streamlines. The dye streams show

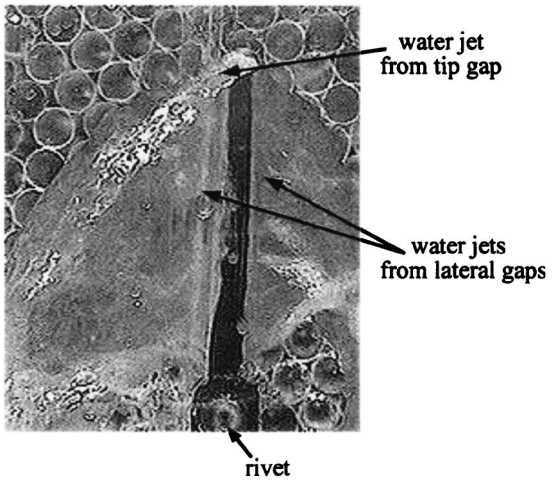

FIG. 4. Front view (see Fig. 2 and Fig. 5) of the water flow around the reed if the water discharge tank is empty. The reed also oscillates in this configuration. Water plane-jets are formed from the lateral and tip gaps. The downstream side of the reed (that is visible in the picture) is in a dry region.

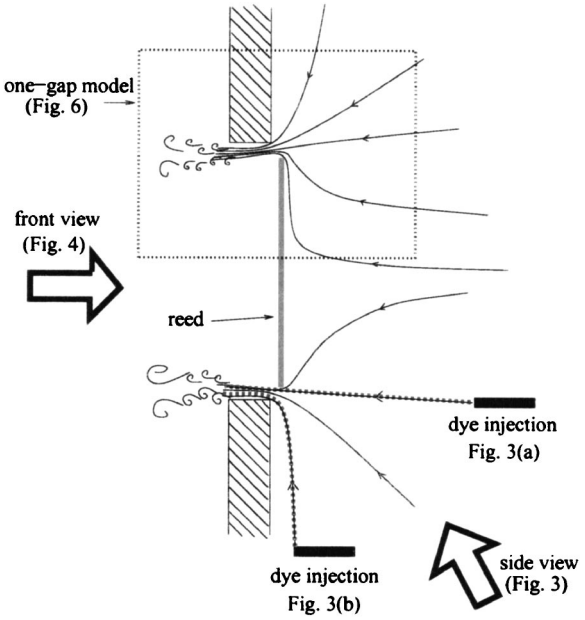

FIG. 5. Sketch of the flow patterns through the reed gaps in a plane $x_3 = \cos t$. The upstream flow is a potential flow induced by the sinks (the lateral gaps). Downstream of each gap, the flow is a plane wall-jet, and it turns to a turbulent free-jet after separation from the exhaust channel walls.

that it is consistent to model the upstream flow by potential sinks. Moreover, for injection points far enough from the tip gap, streamlines lie in planes $x_3 = \text{constant}$, where x_i is the coordinate along the axe $\mathbf{e_i}$ (see Fig. 1). Thus, the flow upstream of the reed seems to be two-dimensional. This assumption is used in the proposed flow model to describe the near-field potential flow. The outflow is turbulent. In photographs, we see the mixing and the diffusion of the dye jets downstream of the reed. However, the characteristic sizes of the turbulent structures are small compared to the reed width h. There are no large coherent vortices that could have been responsible for the reed excitation. Because of the very small gap sizes compared to the reed width and to the thickness of the support plate, the downstream flow does not have the characteristics of a wake. In fact, it appears that the jet is attached to the lateral wall of the exhaust channel.

Figure 4 shows the water flow around the reed if the discharge tank is empty so that the downstream fluid is air. Self-oscillations also occur in this configuration. The added mass effect is reduced in comparison with the first configuration because only one side of the reed is immersed in water. Thus, it is not surprising to find a vibration frequency of 206 Hz that is superior to that obtained when the upstream and downstream fluid is water. The flow view of Fig. 4 shows that the downstream flow can be considered as plane jets, which do not interact with the downstream side of the reed. Even though this configuration is unrealistic, it is interesting because it definitively shows that the downstream flow does not take part in the reed oscillation mechanism.

III. AERODYNAMIC EXCITATION AND REED OSCILLATION

A. Dynamics of the potential flow

The flow visualizations in water show that only the upstream face of the vibrating plate is in contact with the moving fluid. Therefore the excitation force must be evaluated by integrating the aerodynamic pressure fluctuation over the upstream face. The flow through the reed gaps can be supposed incompressible because the Mach and Helmholtz numbers are very small. Even if the downstream jets are turbulent at the exit of the exhaust channel, it can be considered to be laminar and irrotationnal to a certain extent from the gaps. Consequently, potential expressions are used to model the upstream and downstream flows. In this analysis, the inviscid two-dimensional flow is described in a section perpendicular to the length of the reed (plane $x_3 = \text{constant}$). This section is supposed to be far enough from the tip of the reed to avoid three-dimensional effects. Using the superposition property of potential flows,[13] the total flow could be found by the summation of the identical potential flows created by the two lateral gaps drawn in Fig. 5. However, in order to obtain the most simple mathematical expressions, it is reasonable to suppose that the physics of reed excitation can be described considering simply one-gap flow. This very simplified representation of a blown-closed free reed is shown in Fig. 6.

The width of the gap is $e(t) = \sqrt{x_2^2(t) + a^2}$ if $x_2(t) > 0$ and $e(t) = a$ if $x_2(t) < 0$. The flow past the reed is approximated by assuming that the reed lies in the support plate plane $x_2 = 0$. The potential of the upstream flow is expressed as the sum of a continuous distribution of fluid sinks,[13]

$$\phi_1(x_1, x_2, t) = -\frac{1}{\pi} V(t) \int_0^{e(t)} \ln\left(\frac{\sqrt{(x_1 - u)^2 + x_2^2}}{e(t)/2} \right) du, \tag{1}$$

where $V(t)$ is the velocity of the downstream jet. The jet velocity $\mathbf{V_2} = -V(t)\mathbf{e_2}$ is supposed to be constant across the gap, along the axe $\mathbf{e_1}$. The integral of Eq. (1) can be analytically evaluated. The expressions of $\phi_1(x_1, x_2, t)$ and the velocity $\mathbf{V_1}(x_1, x_2, t) = \mathbf{grad}(\phi_1)$ are given in Appendix A. The logarithmic singularity in the expressions of the potential and velocity at points (0,0) and $(e(t),0)$ are a classical consequence of the inviscid potential model. At these points, the

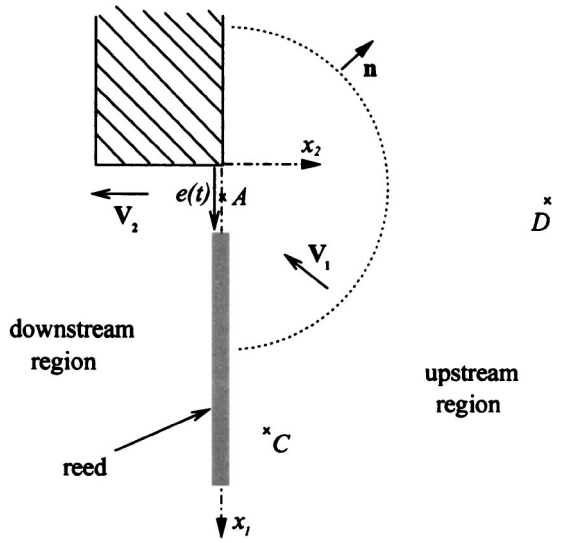

FIG. 6. One-gap simplified model: schematic representation of the reed for aerodynamic and aeroacoustic modeling. ⋯ is the control surface Σ that is used in the aeroacoustic source calculation.

flow separates due to viscous effects. No practical mathematical expressions are available for the description of entire flow with separation. Then, for simplicity the downstream flow potential is chosen in order to ensure the continuity of the potential, velocity and pressure at the center A of the reed opening:

$$\phi_2(x_1,x_2,t) = -V(t)x_2 + \frac{1}{\pi}q(t), \tag{2}$$

where $q(t)=V(t)e(t)$ is the volume flux. This potential describes a laminar jet of velocity $V(t)$. Of course, farther away downstream from the reed gap, the flow is a spreading turbulent jet but there is no need for modeling this region.

The aerodynamic variable of the potential flow must verify the unsteady Bernoulli equation,[13]

$$\frac{\partial\phi(\mathbf{x},t)}{\partial t} + \frac{\|\mathbf{V}(\mathbf{x},t)\|^2}{2} + \frac{P(\mathbf{x},t)}{\rho_0} = C(t), \tag{3}$$

where $P(\mathbf{x},t)$ is the deviation pressure from the atmospheric pressure P_{atm}, ρ_0 is the density of the fluid and $C(t)$ is a constant independent of spatial coordinates but that can depend on time. The value of $C(t)$ can be evaluated by applying the Bernoulli equation at the center A of the reed gap where $x_1^A=e(t)/2$, $x_2^A=0$. At this point, we have $P_A=0$, $\mathbf{V_A}=-V(t)\mathbf{e}_2$ and $\partial\phi_A/\partial t=\partial q/\pi\,\partial t$; then we obtain

$$C(t) = \frac{V^2(t)}{2} + \frac{1}{\pi}\frac{\partial q}{\partial t}. \tag{4}$$

A second application of Eq. (3) at a point B located far away upstream the reed leads to a fundamental equation that expresses the inertial effects of the flow. For the sake of simplicity, we can take the point B at the position $x_1^B=e(t)/2$, $x_2^B \gg e(t)$ where $P_B=P_0$, $\mathbf{V_B}\approx 0$. We can write

$$-K_0(t)\frac{\partial q}{\partial t} + \frac{P_0}{\rho_0} = \frac{V^2(t)}{2}, \tag{5}$$

where $K_0(t)$ is calculated from the expression of the time derivative of the upstream potential [Eq. (A3)]. With the particular choice of point B, we obtain $K_0(t) \approx \ln(2x_2^B/e(t))/\pi$.

This differential equation (5) shows that the time dependence of the orifice flow velocity results from the inertial property of the upstream flow. The choice of the point B appears to be arbitrary and this point is discussed in Sec. V.

B. Aerodynamic pressure force

The pressure on the upstream face of the reed can be found by a third application of the Bernoulli equation. The expression of the aerodynamic pressure for a point such as $e(t)<x_1<e(t)+h$ and $x_2=0$ is

$$\begin{aligned} P(x_1,0,t) = \frac{\rho_0}{2}V^2(t)\left(1-\left(\frac{1}{\pi}\ln\left(\frac{x_1-e(t)}{x_1}\right)\right)^2\right) \\ -\frac{\rho_0}{\pi}\frac{\partial V}{\partial t}x_1\ln\left(\frac{x_1-e(t)}{x_1}\right) \\ +\frac{\rho_0}{\pi}\frac{\partial q}{\partial t}\ln\left(\frac{x_1-e(t)}{e(t)/2}\right). \end{aligned} \tag{6}$$

The total pressure force induced by the one-gap flow dynamics on the upstream side of the reed is

$$\mathbf{F_1}(t) = -\left(\int_{e(t)}^{e(t)+h} P(x_1,0,t)\,dx_1\right)\mathbf{e}_2 \tag{7}$$

or

$$\begin{aligned} F_1(t) = -h\frac{\rho_0}{2}V^2(t)(1-A_1(t)) + \rho_0 h^2 A_2(t)\frac{\partial V}{\partial t} \\ -\rho_0 h A_3(t)\frac{\partial q}{\partial t}. \end{aligned} \tag{8}$$

The expressions of adimensional parameters $A_1(t)$, $A_2(t)$ and $A_3(t)$ are given in Appendix B. The first term on the right hand side of Eq. (8) is the classical so-called Bernoulli force in quasi-stationary modeling. In this term, $A_1(t)$ is the parameter that represents the pressure fluctuations associated with volume flux fluctuations due to the reed aperture variations. This kind of time-dependent contraction parameter is found in all oscillating reed models.[1,5,2,4] It is interesting to note that the force fluctuations induced by the contraction effect are not responsible for the reed excitation mechanism. Indeed, it is possible to show from mathematical expressions given in Appendix B that at the first order, $A_1(t)$, is proportional to $e^2(t)$. Therefore the force associated with the aperture variation is in phase with the reed displacement: it does not transfer energy to the reed motion.

The Bernoulli force also depends on $V^2(t)$. These velocity fluctuations, given by Eq. (5), are generated by the inertial loading of the upstream fluid. The fluid inertia also adds the second and third terms on the right hand side of Eq. (8). The velocity fluctuations due to fluid inertia and the inertial forces are not in phase with the reed displacement.

C. Reed motion and reciprocal flow

It has been previously shown that the motion of a free reed[14,15] is almost perfectly sinusoidal. Laser vibrometer system measurements that are not reported here have also been made on our accordion reeds and the results are consistent with the previous observations. Thus the reed can be modeled by a mass-spring-damping single oscillator system. The reed motion leads to a reciprocal fluid current that is not dependent on the main unsteady flow. The contribution of the reed surface vibration to the total pressure can be studied using the radiation impedance of a baffled rectangular piston $Z_m(\omega)=F_2(\omega)/u(\omega)$, where $u(\omega)$ is the normal velocity of the reed and $F_2(\omega)$ is the reaction force of the fluid back on the driving piston for an angular frequency ω. For $\omega l/c_0 \ll 1$, where c_0 is the speed of sound, the largest term in Z_m is its imaginary part, the reactance. Morse and Ingard[16] calculated the expression of the reactance of a baffled rectangular piston for one of its faces,

$$F_2(\omega)=-i\omega m_f u(\omega), \quad \text{with}$$
$$m_f=\frac{8}{9\pi}\rho_0 lh\frac{l^2+lh+h^2}{l+h}. \tag{9}$$

This force F_2 is in an opposite phase with the reed acceleration and it describes that the fluid entrained by one reed side has an apparent mass of m_f. Consequently, the effective fluid mass $2m_f$ must be added to the accelerated reed mass m in the two-dimensional reed motion equation,

$$\frac{(m+2m_f)}{l}\frac{\partial^2 x_2}{\partial t^2}+\frac{c}{l}\frac{\partial x_2}{\partial t}+\frac{k}{l}(x_2-x_0)=F_1(t), \tag{10}$$

where c and k are the equivalent damping and stiffness of the reed. The added mass causes a decrease of the natural frequency of the reed. In air, this effect is very small but in a heavier fluid such as water the difference between the intrinsic natural frequency and the measured natural frequency can be very large. The reed oscillator coefficients have been determined by a classical experimental procedure based on static stiffness evaluation and free decay behavior. These measurements are not detailed in this paper. The oscillator mass is determined from the measurement of the natural frequency of the reed in air. The experimental effective mass then includes both the intrinsic mass m and the added mass of air $2m_f$. In fact, the study of the reed-induced reciprocal flow is only useful for the estimation of the near-field resultant pressure that is added to the aerodynamic pressure $P_1(t)$ for comparisons with experimental data (Sec. V). In the near field of the upstream region, the mean fluctuating pressure associated with the reed reactance is

$$P_2(t)=-\frac{1}{lh}m_f\frac{\partial^2 x_2}{\partial t^2}. \tag{11}$$

Moreover, it is worth noting that the reciprocal flow associated with the reed reactance must not be taken into account for the calculation of the far-field acoustic pressure.

In this section, we have written in the time domain the equations of flow and reed motion. If we notice that $V(t)$ and $\partial V/\partial t$ can be expressed as a function of $x_2(t)$ and $q(t)$ and their time derivative, we see that the model of reed excitation is a differential system of two coupled nonlinear equations (5) and (10) with the unknowns $x_2(t)$ and $q(t)$. A fourth order Runge–Kutta algorithm is used for the numerical system solving. The nonconstant coefficients of the differential system are updated at each step of the Runge–Kutta procedure.

IV. AEROACOUSTIC MODEL

As for other wind instruments, the sound produced by the accordion is a consequence of the unsteady flow through the reed apertures. But unlike resonator-coupled instruments, we cannot deduce the sound from the analysis of the resonator response to the inlet unsteady flux. For the accordion reed, we can consider that the fluctuating fluid flow acts directly as a source of sound on the free acoustic medium. Therefore we neglect in the model all contributions of reflection or diffraction of acoustic waves on the neighboring solid walls.

A. Lighthill's acoustic analogy

The problem of sound production by flow was first investigated by Lighthill[17] in 1952. His theory is based on the comparison between the exact equations of fluid motion with the equations of sound propagation in a medium at rest. The mass and momentum conservation equations are rewritten to form the most general inhomogeneous wave equation,

$$\frac{\partial^2\rho'}{\partial t^2}-c_0^2\nabla^2\rho'=\frac{\partial^2 T_{ij}(\mathbf{y},t)}{\partial y_i\,\partial y_j} \tag{12}$$

where $\rho'=\rho-\rho_0$ and $p'=p-P_{\text{atm}}$. The tensor $T_{ij}=\rho u_i u_j+(p'-c_0^2\rho')\delta_{ij}-\tau_{ij}$ is the Lighthill stress tensor where δ_{ij} is the Kronecker delta and τ_{ij} is the viscous stress tensor. The summation convention on indices i and j is used. For high Reynolds, low Mach number flows and in the absence of thermal sources the Lighthill stress tensor can be reduced[17] to $T_{ij}\approx\rho_0 u_i u_j$. With this simplification, the source term of Eq. (12) expresses the variation of the rate of momentum flux which is induced by turbulent processes. The upstream sink flow is not turbulent and, arguing that the upstream and downstream acoustic waves are the same but with an opposite sign, it becomes evident that the turbulent sources are not important in the generation of an accordion reed sound for both the blowing and drawing notes. However, the physics of aeroacoustic sources can only be analyzed by using the mathematical expressions of the far acoustic field. The far-field acoustic pressure is calculated using the convolution product of Lighthill's source with the free-space Green's function. In this case, the spatial derivatives of Lighthill's tensor with respect to the source position must be rewritten in terms of derivatives with respect to the observer's position. By a careful mathematical analysis[18,19] of the bounded volume integration of Lighthill's tensor, mass and momentum sources appear as residual terms of the Lighthill tensor flux through the surface that bounds the volume. These monopole and dipole terms on the surface add to the quadrupole source generated by turbulence in the control volume. This analysis was first proposed by Curle,[18] and

Ffowcs Williams and Hawkings[20] gave a rigorous mathematical framework in order to take into account solid or fictitious (permeable) control surfaces and moving solid bodies.

B. Application of the permeable Ffowcs Williams–Hawkings integral method

The Ffowcs Williams–Hawkings (FW–H) integral method[20] was first used for the calculation of noise generated both by turbulence and moving impenetrable surfaces, but recently the FW–H equation has been validated as an integral formulation with permeable surfaces.[21,22]

The derivation of the FW–H formulation is based on the mathematical technique of generalized functions. A generalized function is formed with the aid of Heavisides's function $H(f)$ defined to be unity where $f>0$ and zero where $f<0$. The equation $f=0$ defines the control surface Σ.

The Navier–Stokes equations are written for the generalized density $H(f)\rho'$, momentum $H(f)\rho u_i$, and pressure $H(f)p'$. As for Lighthill's equation (12), an inhomogeneous wave equation can be expressed from the mass and momentum conservation equations. Details of the derivation of the FW–H equation from conservation laws are given by Brentner and Farassat.[23] For a nonmoving permeable surface, the inhomogeneous wave equation is

$$\frac{\partial^2 \rho' H(f)}{\partial t^2} - c_0^2 \nabla^2 \rho' H(f) = \frac{\partial^2 T_{ij} H(f)}{\partial y_i \partial y_j} - \frac{\partial}{\partial y_i}\left((\rho u_i u_j + p\delta_{ij} - \tau_{ij})\delta(f)\frac{\partial f}{\partial y_j}\right) + \frac{\partial}{\partial t}\left(\rho u_j \delta(f)\frac{\partial f}{\partial y_j}\right). \tag{13}$$

Generally, the control surface Σ is supposed to enclose all the volume sources described by Lighthill's tensor T_{ij}. Then, $T_{ij}H(f)=0$ for $f\geqslant 0$. Moreover, as the free-field Green's function is used for the calculation of the far-field acoustic pressure, all the possible flow/acoustic interactions and acoustic wave reflections on solid walls must be taken into account as flow variables on the control surface. Because of our incompressible approach, all these effects are neglected in the source terms. Finally, neglecting the viscous stress tensor in the second term of the right hand side of the FW–H equation, we see that the acoustic sources can be divided into a monopole Q and a dipole F_i that are calculated on the permeable control surface,

$$Q(\mathbf{y},t) = \rho u_j \frac{\partial f}{\partial y_j} \approx \rho_0 u_j \frac{\partial f}{\partial y_j}, \tag{14}$$

$$F_i(\mathbf{y},t) = -(\rho u_i u_j + p\delta_{ij})\frac{\partial f}{\partial y_j} \approx -(\rho_0 u_i u_j + p\delta_{ij})\frac{\partial f}{\partial y_j}. \tag{15}$$

The free-field solution of Eq. (13) is the convolution product of the source terms with the free-space Green's function. After rearrangement of the integral expressions (see Appendix C), the density fluctuations are given by

$$\rho'(\mathbf{x},t) = \frac{1}{4\pi c_0^2}\frac{\partial}{\partial x_i}\int_\Sigma \left[\frac{\rho_0 u_i u_j + p\delta_{ij}}{r}\right] n_j \, d\Sigma + \frac{1}{4\pi c_0^2}\frac{\partial}{\partial t}\int_\Sigma \left[\frac{\rho_0 u_j}{r}\right] n_j \, d\Sigma, \tag{16}$$

where the square brackets denote that the functions are evaluated at the retarded time $\tau = t - r/c_0$ and n_j are the components of the unit outward normal vector to surface. When $|\mathbf{x}| \ll L \ll \lambda$, where L is a typical dimension of the control surface Σ and λ is a typical wavelength of the sound generated, a classical simplification procedure[18,17] leads to the final expression of the acoustic pressure,

$$p_{ac}(\mathbf{x}, t+|\mathbf{x}|/c_0) = \frac{1}{4\pi c_0}\frac{x_i}{|\mathbf{x}|^2}\frac{\partial}{\partial t}\int_\Sigma (\rho_0 u_i u_j + p\delta_{ij}) n_j \, d\Sigma + \frac{\rho_0}{4\pi|\mathbf{x}|}\frac{\partial}{\partial t}\int_\Sigma u_j n_j \, d\Sigma. \tag{17}$$

Obviously, the second integral on the right hand side of Eq. (17) is the expression of the total volume flux through the control surface that is evidently equal to $q(t)$. The first source term of Eq. (17) has a dipolar form and its value is evaluated numerically using an adaptive recursive Simpson's rule.

V. EXPERIMENTS AND MODEL VALIDATION

A. Experimental study in air

The experimental setup for air measurements is similar to that used for water visualizations (Fig. 2). The water supply tank is replaced by a low-impedance pressure source that insures a constant blowing pressure inside the reservoir. A probe microphone measures the aerodynamic pressure at a few millimeters from the upstream face of the reed. A variable capacitance transducer is used for the motion of the reed. This transducer is based on a condenser microphone, the membrane of which is electrically replaced by the reed. A water manometer measures the average supply pressure and a microphone captures the radiated sound. This microphone is located at 25 cm downstream of the reed.

In Fig. 7, displacement, aerodynamic pressure and acoustic pressure are represented for a reed with a natural frequency of $f_0 = 795$ Hz. The characteristic dimensions of the valve are $l = 22.9$ mm, $h = 2.5$ mm, $a = 0.14$ mm, and $x_0 = 0.2$ mm. The supply pressure is $P_0 = 40$ Pa. As expected, we see in Fig. 7(a) that the reed motion is composed of sinusoidal oscillations around a displaced equilibrium position. We note that for low playing pressure, the steady displacement of the reed is small and we can consider that the equilibrium position is about x_0. Figure 7(b) shows a sharp aerodynamic pressure spike at the moment when the reed enters the slot. Since the equilibrium position is not so far from the plane $x_2 = 0$, the force induced by this strong pressure variation is nearly in phase with the reed velocity. Thus, it provides energy to the oscillator. Similarly at the reed opening, a negative pressure variation occurs but it is less violent. The downstream acoustic signal shown in Fig. 7(c)

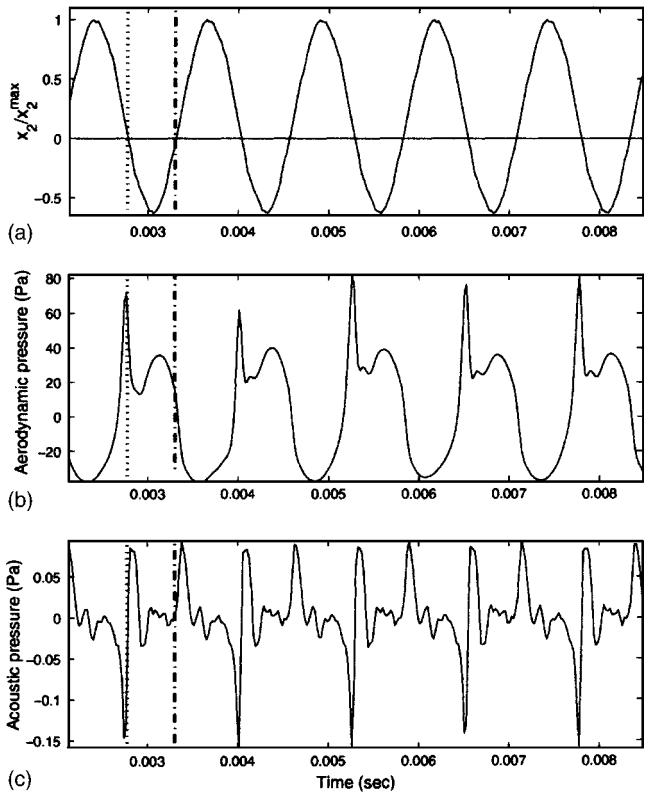

FIG. 7. Experimental measurements in air flow: (a) reed displacement; (b) upstream aerodynamic pressure; (c) downstream acoustic pressure. ···, closing of the valve; –·–, opening of the valve.

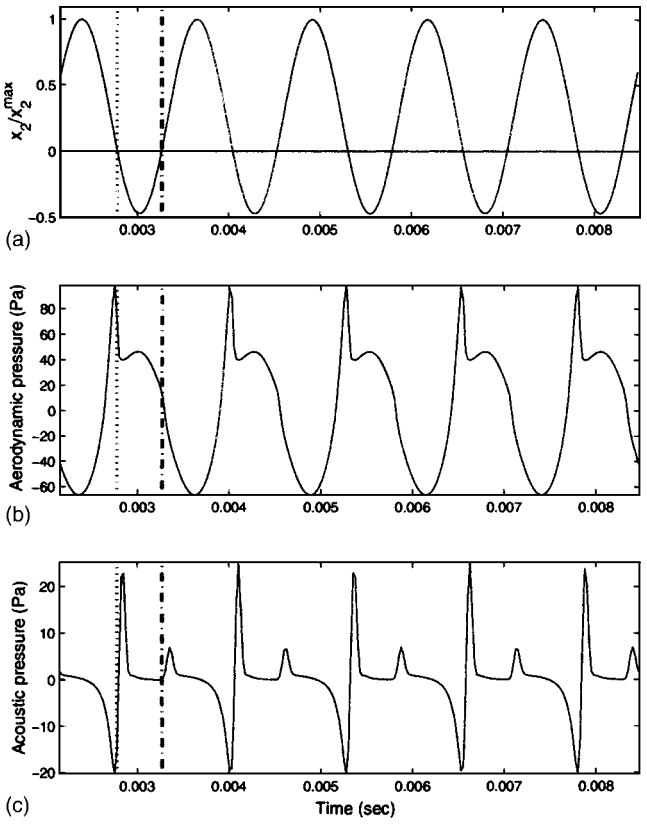

FIG. 9. Results of the model calculation: (a) reed displacement; (b) aerodynamic pressure at point C; (c) reverse of the acoustic waveform at point D. ···, closing of the valve; –·–, opening of the valve.

greatly differs from the aerodynamic pressure waveform. This illustrates the complex conversion mechanism of the fluid mechanical energy into acoustic energy. Only the sharp pressure spike associated with the reed closure is common to the two waveforms with an opposite sign. This reverse sign results from the quasi-symmetry of the upstream and downstream flow with regard to the aperture plane. Figure 8 shows the spectrum of the acoustic pressure. In the rich spectral distribution of the reed sound, the odd harmonics are predominant. It is interesting to note that both the waveform and spectrum of the acoustic signal compare well with signals extracted from recordings of accordion notes.[24]

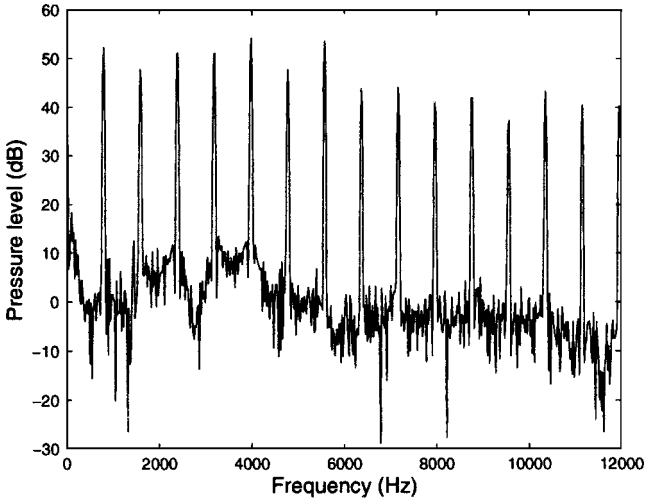

FIG. 8. Spectrum of the measured acoustic pressure.

B. Application of the model

For the calculation, the model variables are initialized at zero and the reed position is set to x_0. The differential equation system, Eqs. (5) and (10), is solved using Eq. (8) for the excitation force. After the transient, self-sustained sinusoidal oscillations are observed at the natural frequency of the reed [see Fig. 9(a)]. Using the computed fluid variables $q(t)$ and $V(t)$, the aerodynamic pressure at point C of Fig. 6 is computed from the Bernoulli equation (3) with the complete expression of the potential derivative, Eq. (A3). For a comparison with the probe microphone signal, the contribution $P_2(t)$ of the reciprocal flow is added to this aerodynamic excitation pressure. The total signal is plotted in Fig. 9(b). The agreement with the measured waveform is good.

Since the downstream flow model is very simplified compared to the actual development of turbulent spreading jets, the acoustic pressure is calculated in the upstream region. The symmetry property of the produced sound is used to compare the calculated signal to the acoustic measurement performed in the downstream region. The modeled acoustic pressure is the external acoustic pressure that would be measured if the reed oscillated in its sucking configuration. The fluid variables calculated on the control surface Σ defined in Fig. 6 are introduced in the integral equation (17). The result is plotted in Fig. 9(c). Even if the pressure spike occurring just after the reed opening is smaller than the measured one,

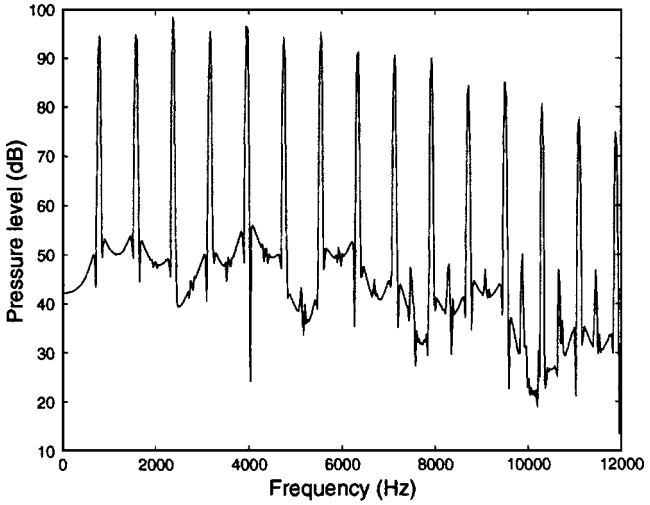

FIG. 10. Spectrum of the modeled acoustic pressure.

the modeled waveform reproduces quite well the experimental acoustic signal. Moreover, it is shown in Fig. 10 that the odd harmonics of the modeled sound spectrum are more powerful than the even ones, which is a characteristic of the accordion reed sound. Examples of synthetized sounds are available on the IRCAM website.[25]

C. Analysis of the aerodynamic excitation

From the previous comparisons, we can suppose that the physics of both reed excitation and acoustic emission are well reproduced by the model. The calculation results can be used to highlight some details of the physical mechanisms.

For example, Fig. 11 shows the components of the aerodynamic pressure force $F_1(t)$ associated with the Bernoulli force [the first term of Eq. (8)] and inertial force [second and third terms of Eq. (8)]. This figure clearly demonstrates that the inertial force is a negligible part of the total force. In most reed models,[1,5,2,4] inertial forces are neglected. This simplification can also be done for the accordion reed model and from Eq. (8), the average excitation pressure on the upstream face of the reed is now

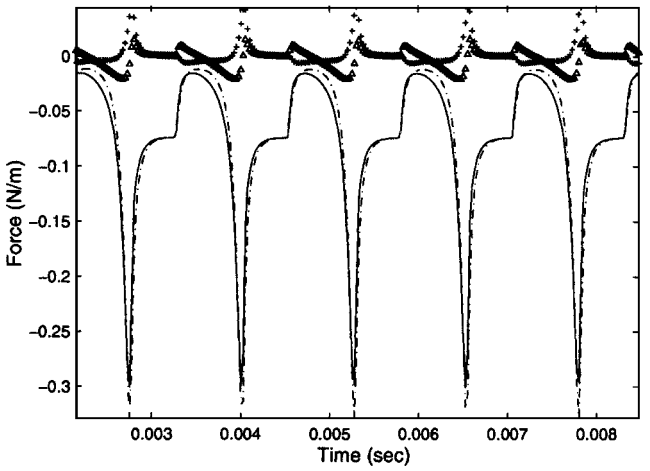

FIG. 11. A comparison of the three terms of the aerodynamic force given by Eq. (8): $-\cdot-$, first term; $\triangle$, second term; $+$, third term; $-$, total force.

$$\langle P_1(t)\rangle = -\frac{1}{h}F_1(t) = \frac{\rho_0}{2}V^2(t)(1-A_1(t)). \tag{18}$$

Replacing the fluid velocity in Eq. (18) by its expression given by Eq. (5), the average pressure becomes

$$\langle P_1(t)\rangle = -\rho_0 K_0(t)(1-A_1(t))\frac{\partial q}{\partial t} + P_0(1-A_1(t)). \tag{19}$$

As explained before, the contraction effect associated with $A_1(t)$ does not contribute to the excitation mechanism. Thus, the term $P_0(1-A_1(t))$ on the right hand side of Eq. (19) is not an excitation pressure. Finally, the expression of the excitation pressure is

$$\langle P_1(t)\rangle_{exc} = -\rho_0 K_0(t)(1-A_1(t))\frac{\partial q}{\partial t}. \tag{20}$$

This relation looks like an impedance relation giving the pressure as a function of the volume flux. In this case, the impedance is inertial. The value of the equivalent ''acoustic'' inertia $M(t)=\rho_0 K_0(t)(1-A_1(t))$ is time-dependent.

Unlike traditional theoretical approaches of oscillating valves[1] based on acoustic impedances of upstream and downstream volumes, Eq. (20) is related to the impedance of the orifice. $M(t)$ can be interpreted as the mass end correction[16] of the upstream side of the gap. The mass end correction depends on the detailed form of the potential flow and gap geometry. Thus, the time dependence of $M(t)$ is due to the variation of gap size. In particular, $K_0(t)$ is related to the total quantity of fluid that takes part in the inertial mechanism. For the calculation presented in this paper, the average value of the parameter K_0 is 4.5. This corresponds to a very large distance of the reference point B where the pressure is supposed to be constant and the fluid velocity is zero. The choice of point B is arbitrary but first applications of the aerodynamic model show that the influence of K_0 on the result becomes small above a certain value that depends on dimensions and characteristics of the simulated reed.

D. Analysis of the sound production

In addition, the presented model allows us to analyze the mechanism of sound production. The monopole and dipole sources of Eq. (17) are represented in Fig. 12. It appears immediately that the sound of the reed is dominated by the dipolar component. This observation is in opposition to the physics of the reed coupled to a resonator. Indeed, as mentioned in the Introduction, the acoustic source exciting the air column of the resonator is modeled as the variation of the volume flux through the reed gaps. In the case of a free reed, the monopolar source associated with unsteady volume flux at the orifice is negligible, the acoustic waves are excited by the violent changes of momentum flux through the orifice.

VI. CONCLUSIONS

In this paper, a simplified representation of a blown-closed reed used, for example, in accordions has been studied. The flow around the reed is described using an incompressible potential flow theory and the excitation force in this

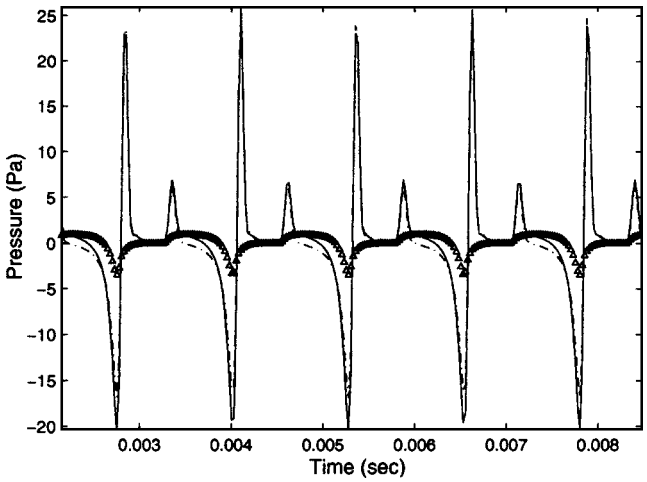

FIG. 12. A comparison of the monopole and dipole terms of the acoustic expression, Eq. (17): △, monopole term; –·–, dipole term; —, total aeroacoustic source.

model is associated with the inertial load of the upstream fluid. The delay in the variation of upstream fluid velocity due to the inertia leads to a velocity fluctuation in the reed opening. Unlike for resonator-coupled reeds, the pressure–velocity relationship is not driven by the impedance of upstream and downstream volumes but by an equivalent inertial impedance of the gaps. One of the difficulties arises from the time-dependence of the orifice geometry which leads to a time-dependent mass inertia.

This work also provides the first model of the source of sound generated by a free reed in the absence of a resonator. Despite the numerous simplifications made in the calculation, the qualitative agreement of the synthesized pressure signal with the measured one in terms of waveform and spectrum is quite good. The model is based on the application of an acoustic analogy that allows the derivation of the acoustic pressure in the far-field as a function of the aerodynamic variables known in the source region. In our case, the acoustic source is calculated in the time domain but it is also possible to perform the calculation in the frequency domain.

ACKNOWLEDGMENTS

The authors wish to thank Agnès Maurel and Philippe Petitjeans of the Ecole Supérieure de Physique et de Chimie Industrielles for helpful discussions about the flow visualization arrangement. We also want to thank Alain Terrier and Gérard Bertrand of IRCAM for their help in the measurements.

APPENDIX A: CALCULATION OF THE UPSTREAM FLOW

In this appendix, the analytical expressions of the flow potential and velocity for the upstream region are given.

1. Flow potential in the upstream region

The upstream potential is given by Eq. (1):

$$\phi_1(x_1,x_2,t) = -\frac{1}{\pi} V(t) \int_0^{e(t)} \ln\left(\frac{\sqrt{(x_1-u)^2+x_2^2}}{e(t)/2} \right) du. \tag{A1}$$

The coordinates x_1 and x_2 are given in Fig. 6. $V(t)$ is the fluid velocity through the gap and $e(t)$ is the gap size. After calculations, one can obtain the explicit expression of the potential:

$$\begin{aligned}\phi_1(x_1,x_2,t) = -\frac{1}{\pi} V(t) \Bigg(& \frac{1}{2} e(t) \ln\left(\frac{(x_1-e(t))^2+x_2^2}{(e(t)/2)^2} \right) \\ & - \frac{1}{2} x_1 \ln\left(\frac{(x_1-e(t))^2+x_2^2}{x_1^2+x_2^2} \right) + x_2 \Bigg(\arctan\left(\frac{x_1}{x_2} \right) \\ & - \arctan\left(\frac{x_1-e(t)}{x_2} \right) \Bigg) \Bigg) + \frac{1}{\pi} q(t), \end{aligned} \tag{A2}$$

where $q(t)=V(t)e(t)$ is the volume flux through the gap.

2. Time derivative of the flow potential in the upstream region

The time derivative of the flow potential given by Eq. (A2) is

$$\begin{aligned}\frac{\partial \phi_1(x_1,x_2,t)}{\partial t} = & \frac{1}{\pi} \frac{\partial V}{\partial t} \Bigg(\frac{1}{2} x_1 \ln\left(\frac{(x_1-e(t))^2+x_2^2}{x_1^2+x_2^2} \right) \\ & - x_2 \Bigg(\arctan\left(\frac{x_1}{x_2} \right) - \arctan\left(\frac{x_1-e(t)}{x_2} \right) \Bigg) \Bigg) \\ & + \frac{1}{\pi} \frac{\partial q}{\partial t} \left(1 - \ln\left(\frac{\sqrt{(x_1-e(t))^2+x_2^2}}{e(t)/2} \right) \right). \end{aligned} \tag{A3}$$

3. Components of the velocity vector in the upstream region

The two components of the upstream velocity vector are found by calculating the gradient of the potential ϕ_1 [Eq. (A2)]:

$$V_{1,x_1}(x_1,x_2,t) = \frac{\partial \phi_1}{\partial x_1} = \frac{V(t)}{2\pi} \ln\left(\frac{(x_1-e(t))^2+x_2^2}{x_1^2+x_2^2} \right), \tag{A4}$$

$$\begin{aligned} V_{1,x_2}(x_1,x_2,t) &= \frac{\partial \phi_1}{\partial x_2} \\ &= \frac{V(t)}{\pi} \left(\arctan\left(\frac{x_1-e(t)}{x_2} \right) - \arctan\left(\frac{x_1}{x_2} \right) \right). \end{aligned} \tag{A5}$$

APPENDIX B: EXPRESSION OF THE AERODYNAMIC FORCE

The total force on the upstream face of the reed is given by integration of the aerodynamic pressure [Eq. (6)] over the reed width h,

$$\mathbf{F_1}(t) = -\left(\int_{e(t)}^{e(t)+h} P(x_1,0,t)\, dx_1 \right) \mathbf{e}_2. \tag{B1}$$

The force then has the form

$$F_1(t) = -h\frac{\rho_0}{2}V^2(t)(1-A_1(t)) + \rho_0 h^2 A_2(t)\frac{\partial V}{\partial t} - \rho_0 h A_3(t)\frac{\partial q}{\partial t}, \tag{B2}$$

with the parameters

$$A_1(t) = \frac{1}{h\pi^2}\int_{e(t)}^{e(t)+h}\left(\ln\left(\frac{x_1 - e(t)}{x_1}\right)\right)^2 dx_1, \tag{B3}$$

$$A_2(t) = \frac{1}{h^2\pi}\int_{e(t)}^{e(t)+h} x_1 \ln\left(\frac{x_1 - e(t)}{x_1}\right) dx_1, \tag{B4}$$

$$A_3(t) = \frac{1}{h\pi}\int_{e(t)}^{e(t)+h}\ln\left(\frac{x_1 - e(t)}{e(t)/2}\right) dx_1. \tag{B5}$$

For an analytical calculation of the integrals, we can note that the logarithmic singularities in potential and velocity expressions are integrable.

The final expressions of the parameters A_1, A_2, and A_3 are given below.

1. Parameter $A_1(t)$

$$A_1(t) = \frac{1}{\pi^2}\left(\ln^2(h) + \left(1+\frac{e(t)}{h}\right)\ln(e(t)+h) \times \ln\left(\frac{e(t)+h}{h^2}\right) + \frac{e(t)}{h}\ln(e(t))\ln\left(\frac{e(t)}{h^2}\right) - 2\frac{e(t)}{h}\,\mathrm{dilog}\left(\frac{e(t)+h}{e(t)}\right)\right), \tag{B6}$$

where the dilogarithm function is defined by

$$\mathrm{dilog}(x) = \int_1^x \frac{\ln(u)}{1-u}du. \tag{B7}$$

2. Parameter $A_2(t)$

$$A_2(t) = \frac{1}{2\pi}\left(\ln(h) + \frac{e(t)}{h}(\ln(h^2)-1) + \frac{e^2(t)}{h^2}\ln(e(t)) - \frac{(e(t)+h)^2}{h^2}\ln(e(t)+h)\right). \tag{B8}$$

3. Parameter $A_3(t)$

$$A_3(t) = \frac{1}{\pi}\left(\ln\left(\frac{2h}{e(t)}\right) - 1\right). \tag{B9}$$

APPENDIX C: CALCULATION OF THE ACOUSTIC DENSITY FLUCTUATIONS

The free-field Green's function is

$$G(\mathbf{x},t|\mathbf{y},\tau) = \frac{1}{4\pi c_0^2 r}\delta(g), \quad \text{with } g = \tau - t + r/c_0, \quad r = \|\mathbf{x}-\mathbf{y}\|. \tag{C1}$$

where $\mathbf{y}$ is a point in the source region and $\mathbf{x}$ is the observer's position. Then the acoustic density fluctuations are

$$\rho'(\mathbf{x},t)H(f) = \frac{1}{4\pi c_0^2}\int_{\mathcal{R}^3}\int_{\mathcal{R}}\frac{1}{r}\left(\frac{\partial}{\partial y_i}F_i(\mathbf{y},t)\,\delta(f)\right)\delta(g)\,\mathbf{d}\tau\,d\mathbf{y} + \frac{1}{4\pi c_0^2}\int_{\mathcal{R}^3}\int_{\mathcal{R}}\frac{1}{r}\frac{\partial}{\partial t}(Q(\mathbf{y},t)\,\delta(f))\delta(g)\,d\tau\,d\mathbf{y}. \tag{C2}$$

The spatial integral of the first term can be developed as

$$\int_{\mathcal{R}^3}\frac{1}{r}\left(\frac{\partial}{\partial y_i}F_i(\mathbf{y},t)\,\delta(f)\right)\delta(g)\,d\mathbf{y} = \int_{\mathcal{R}^3}\frac{\partial}{\partial y_i}\left(\frac{1}{r}F_i(\mathbf{y},t)\,\delta(f)\,\delta(g)\right)d\mathbf{y} - \int_{\mathcal{R}^3}F_i(\mathbf{y},t)\,\delta(f)\frac{\partial}{\partial y_i}\left(\frac{1}{r}\,\delta(g)\right)d\mathbf{y}. \tag{C3}$$

The first integral of the right hand side is zero and noting that $\partial(\delta(g)/r)/\partial y_i = \partial(\delta(g)/r)/\partial x_i$ we can write

$$\int_{\mathcal{R}^3}\frac{1}{r}\left(\frac{\partial}{\partial y_i}F_i(\mathbf{y},t)\,\delta(f)\right)\delta(g)\,d\mathbf{y} = -\frac{\partial}{\partial x_i}\int_{\mathcal{R}^3}\frac{1}{r}F_i(\mathbf{y},t)\,\delta(f)\,\delta(g)\,d\mathbf{y} = \frac{\partial}{\partial x_i}\int_{\Sigma}\frac{1}{r}(\rho_0 u_i u_j + p\,\delta_{ij})n_j\,\delta(g)\,d\Sigma, \tag{C4}$$

with

$$n_j = \frac{1}{|\boldsymbol{\nabla} f|}\frac{\partial f}{\partial y_j}. \tag{C5}$$

The second spatial integral of the density fluctuations can be also written as

$$\int_{\mathcal{R}^3}\frac{1}{r}\frac{\partial}{\partial t}(Q(\mathbf{y},t)\,\delta(f))\,\delta(g)\,d\mathbf{y} = \frac{\partial}{\partial t}\int_{\Sigma}\frac{1}{r}\rho_0 u_j\,\delta(g)\,n_j\,d\Sigma. \tag{C6}$$

Finally, the temporal integration of the two transformed expressions of the spatial integrals immediately gives the formulation of Eq. (16).

[1] N. H. Fletcher, "Autonomous vibration of simple pressure-controlled valves in gas flows," J. Acoust. Soc. Am. **93**, 2172–2180 (1993).

[2] J. Saneyoshi, H. Teramura, and S. Yoshikawa, "Feedback oscillations in reed woodwind and brasswind instruments," Acustica **62**, 194–210 (1987).

[3] S. C. Thompson, "The effect of the reed resonance on woodwind tone production," J. Acoust. Soc. Am. **66**, 1299–1307 (1979).

[4] R. T. Schumacher, "*Ab initio* calculations of the oscillations of a clarinet," Acustica **48**, 71–85 (1981).

[5] A. Hirschberg, R. W. A. van de Laar, J. P. Marrou-Maurières, A. P. J. Wijnands, H. J. Dane, S. G. Kruijswijk, and A. J. M. Houtsma, "A quasi-stationary model of air flow in the reed channel of a single-reed woodwind instruments," Acustica **70**, 146–154 (1990).

[6] B. Gazengel, J. Gilbert, and N. Amir, "Time domain simulation of single reed wind instrument. From the measured input impedance to the synthesis signal. Where are the traps?," Acta Acust. (Beijing) **3**, 445–472 (1995).

[7] J. Gilbert, J. Kergomard, and E. Ngoya, "Calculation of the steady-state

oscillations of a clarinet using the harmonic balance technique,'' J. Acoust. Soc. Am. **86**, 35–41 (1989).
[8] I. R. Titze, ''The physics of small-amplitude oscillation of the vocal folds,'' J. Acoust. Soc. Am. **83**, 1536–1552 (1988).
[9] X. Pelorson, A. Hirschberg, R. R. van Hassel, and A. P. J. Wijnands, ''Theoretical and experimental study of quasisteady-flow separation within the glottis during phonation. Application to a modified two-mass model,'' J. Acoust. Soc. Am. **96**, 3416–3431 (1994).
[10] R. D. Blevins, *Flow-Induced Vibration* (Krieger, Malabar, Florida, 1986).
[11] A. O. St. Hilaire, T. A. Wilson, and G. S. Beavers, ''Aerodynamic excitation of the harmonium reed,'' J. Fluid Mech. **49**, 803–816 (1971).
[12] A. Z. Tarnopolsky, J. C. S. Lai, and N. H. Fletcher, ''Flow structures generated by pressure-controlled self-oscillating reed valves,'' J. Sound Vib. **247**, 213–226 (2001).
[13] A. R. Paterson, *A First Course in Fluid Dynamics* (Cambridge University Press, Cambridge, 1983), pp. 205–242.
[14] J. P. Cottingham, C. J. Lilly, and C. H. Reed, ''The motion of air-driven free reeds,'' *Proceedings of the 2nd Convention of the European Acoustics Association: Forum Acusticum*, Berlin, 1999.
[15] L. Millot, C. Cuesta, and C. Valette, ''Experimental results when playing chromatically on a diatonic harmonica,'' Acustica **87**, 262–270 (2001).
[16] P. M. Morse and K. U. Ingard, *Theoretical Acoustics* (McGraw-Hill, New York, 1968).
[17] M. J. Lighthill, ''On sound generated aerodynamically. I. General theory,'' Proc. R. Soc. London, Ser. A **221**, 564–587 (1952).
[18] N. Curle, ''The influence of solid boundaries upon aerodynamic sound,'' Proc. R. Soc. London, Ser. A **321**, 505–514 (1955).
[19] A. P. Dowling and J. E. Ffowcs Williams, *Sound and Sources of Sound* (Hellis Horwood, Chichester, 1983), pp. 157–166.
[20] J. E. Ffowcs Williams and D. L. Hawkings, ''Sound generation by turbulence and surfaces in arbitrary motion,'' Philos. Trans. R. Soc. London, Ser. A **264**, 321–342 (1969).
[21] P. di Francescantonio, ''A new boundary integral formulation for the prediction of sound radiation,'' J. Sound Vib. **202**, 491–509 (1997).
[22] X. Gloerfelt, C. Bailly, and D. Juvé, ''Computation of the noise radiated by a subsonic cavity using direct simulation and acoustic analogy,'' AIAA Paper No. 2001-2226, 2001.
[23] K. S. Brentner and F. Farassat, ''An analytical comparison of the acoustic analogy and Kirchhoff formulation for moving surface,'' AIAA J. **36**, 1379–1386 (1998).
[24] N. Misdariis, D. Ricot, and R. Caussé, ''Modélisation physique de la vibration d'une anche d'accordéon,'' *Proceedings of the 5th French Congress on Acoustics*, Lausanne, 2000, pp. 281–283.
[25] http://www.ircam.fr/equipes/instruments/ website: last time viewed by the authors: November 2004.